



Publication Year	2022
Acceptance in OA @INAF	2023-02-06T15:09:51Z
Title	Grammage of cosmic rays in the proximity of supernova remnants embedded in a partially ionized medium
Authors	Recchia, S.; GALLI, Daniele; NAVA, Lara; PADOVANI, Marco; Gabici, S.; et al.
DOI	10.1051/0004-6361/202142558
Handle	http://hdl.handle.net/20.500.12386/33191
Journal	ASTRONOMY & ASTROPHYSICS
Number	660

Grammage of cosmic rays in the proximity of supernova remnants embedded in a partially ionized medium

S. Recchia^{1,2*} D. Galli³ L. Nava⁴ M. Padovani³ S. Gabici⁵ A. Marcowith⁶
V. Ptuskin⁷ G. Morlino³

¹*Dipartimento di Fisica, Università di Torino, via P. Giuria 1, 10125 Torino, Italy*

²*Istituto Nazionale di Fisica Nucleare, Sezione di Torino, Via P. Giuria 1, 10125 Torino, Italy*

³*INAF–Osservatorio Astronomico di Arcetri, Largo E. Fermi 5, 50125 Firenze, Italy*

⁴*INAF–Osservatorio Astronomico di Brera, Via Bianchi 46, I-23807 Merate, Italy*

⁵*Université de Paris, CNRS, Astroparticule et Cosmologie, F-75006 Paris, France*

⁶*Laboratoire Univers et particules de Montpellier, Université Montpellier/CNRS, F-34095 Montpellier, France*

⁷*Pushkov Institute of Terrestrial Magnetism, Ionosphere and Radiowave Propagation, 108840, Troitsk, Moscow, Russia*

Accepted XXX. Received YYY; in original form ZZZ

ABSTRACT

We investigate the damping of Alfvén waves generated by the cosmic ray resonant streaming instability in the context of the cosmic ray escape and propagation in the proximity of supernova remnants. We consider ion-neutral damping, turbulent damping and non linear Landau damping in the warm ionized and warm neutral phases of the interstellar medium. For the ion-neutral damping, up-to-date damping coefficients are used. We investigate in particular whether the self-confinement of cosmic rays nearby sources can appreciably affect the grammage. We show that the ion-neutral damping and the turbulent damping effectively limit the residence time of cosmic rays in the source proximity, so that the grammage accumulated near sources is found to be negligible. Contrary to previous results, this also happens in the most extreme scenario where ion-neutral damping is less effective, namely in a medium with only neutral helium and fully ionized hydrogen. Therefore, the standard picture, in which CR secondaries are produced during the whole time spent by cosmic rays throughout the Galactic disk, need not to be deeply revisited.

Key words:

1 INTRODUCTION

The most popular hypothesis for the origin of Galactic cosmic rays (CRs) invokes supernova remnants (SNRs) as the main sources of such particles (see e.g. Blasi 2013; Gabici et al. 2019). In this scenario, which in the last decades had become a paradigm, CR diffusion plays a central role. Diffusion is the key ingredient at the base of the diffusive shock acceleration of particles at SNRs (e.g. Drury 1983). Diffusion also affects the escape of CRs from the acceleration site and the subsequent propagation in the source region, with prominent implications for γ -ray observations (Aharonian & Atoyan 1996; Gabici et al. 2009; Casanova et al. 2010; Ohira et al. 2011; Nava & Gabici 2013). Finally, diffusion determines the confinement time of CRs in the Galaxy, thus affecting the observed spectrum and the abundances of secondary spallation nuclei and of unstable isotopes (Ptuskin & Soutoul 1998; Wiedenbeck et al. 2007).

The diffusion of CRs is thought to be mostly due to the resonant scattering off plasma waves whose wavelength is comparable to the particle’s Larmor radius $r_L = m_p c^2 / eB$, where m_p is the proton mass, B is the magnetic field strength and γ the Lorentz factor (see e.g. Skilling 1975a). The magneto-hydrodynamic (MHD) turbulence relevant for CR propagation is composed of incompressible Alfvénic and compressible (fast and slow) magnetosonic fluctuations (Cho & Lazarian 2002; Fornieri et al. 2021). MHD turbulence is ubiquitous in the interstellar space and may be injected by astrophysical sources (see e.g. Mac Low & Klessen (2004)) but also by CRs themselves. The active role of CRs in producing the waves responsible for their scattering has been widely recognized (see e.g. Wentzel 1974; Skilling 1975b; Cesarsky 1980; Amato 2011). In fact, spatial gradients in the CR density, as those found in the source vicinity, lead to the excitation of Alfvén waves at the resonant scale (Ptuskin et al. 2008). This process, called *resonant streaming instability*, produces waves that propagate along magnetic field lines in the direction of decreasing CR density.

* E-mail: sarah.recchia@unito.it

The density of Alfvén waves that scatter CRs is limited by several damping processes. The most relevant are: (i) ion-neutral damping in a partially ionized medium (Kulsrud & Pearce 1969; Kulsrud & Cesarsky 1971; Zweibel & Shull 1982); (ii) turbulent damping, due to the interaction of a wave with counter-propagating Alfvén wave packets. Such waves may be the result of a background turbulence injected on large scales and cascading to the small scales (we indicate this damping as FG, after Farmer & Goldreich 2004); (iii) non-linear Landau (NLL) damping, due to the interaction of background thermal ions with the beat of two interfering Alfvén waves (see e.g. Felice & Kulsrud 2001; Wiener et al. 2013). The relative importance of these effects depends significantly on the physical conditions and chemical composition of the ambient medium. A few other collisionless and collisional damping processes can impact magnetohydrodynamical wave propagation in a partially ionized gas but they mostly affect high-wavenumber perturbations (Yan & Lazarian 2004). Recently, it has been suggested that dust grains may also contribute to the damping of Alfvén waves (Squire et al. 2021).

In this paper we investigate the escape of CRs from SNRs, and their subsequent self confinement in the source region, as due to the interplay between the generation of Alfvén waves by CR streaming instability, and the damping process mentioned above. Our main goal is to establish whether the self-confinement of CRs nearby sources can appreciably affect the grammage accumulated by these particles. In fact, if this is the case, a significant fraction of CR secondaries would be produced in the vicinity of CR sources, and not during the time spent by CRs in the Galactic disk, as commonly assumed. This would constitute a profound modification of the standard view of CR transport in the Galaxy (see, e.g. D’Angelo et al. 2016). In particular, we focus on the CR propagation in partially ionized phases of the interstellar medium (ISM), showing that the ion-neutral and FG damping can significantly affect the residence time of CRs nearby their sources. We find that, for typical conditions, the grammage accumulated by CRs in the vicinity of sources is negligible compared to that accumulated during the time spent in the Galaxy. Even in the case of a medium made of fully ionized H and neutral He, the combination of ion-neutral and turbulent damping can substantially affect the confinement time¹.

This paper is organized as follows: in Sec. 2 we describe the damping of Alfvén waves by ion-neutral collisions in various partially ionized phases of the ISM, and by other damping mechanisms; in Sec. 3 we illustrate the equations and the setup of our model of CR escape and propagation in the proximity of SNRs, the time dependent CR spectrum and diffusion coefficient, the residence time of CRs in the source proximity and the implications on the grammage; in Sec. 4 we describe our results; and finally in Sec. 5 we draw our conclusions.

¹ The case of a fully neutral (atomic or partially molecular) medium and of a diffuse molecular medium (see, e.g. Brahimi et al. 2020) are not treated here, since the filling factor of such phases is small, but we report the ion-neutral damping rate for such media for the sake of completeness. The case of a fully ionized medium has been extensively treated by Nava et al. (2019).

2 DAMPING OF ALFVÉN WAVES

2.1 Ion-neutral damping

The Galaxy is composed, for most of its volume, by three ISM phases, namely the warm neutral medium (WNM, filling factor $\sim 25\%$), warm ionized medium (WIM, filling factor $\sim 25\%$) and hot ionized medium (HIM, filling factor $\sim 50\%$, see e.g. Ferrière 2001; Ferrière 2019). The physical characteristics of these phases are summarised in Table 1 (from Jean et al. 2009, see also Ferrière 2001; Ferrière 2019). The physical characteristics of the cold neutral medium (CNM) and the diffuse medium (DiM) are also listed for completeness, while their filling factor is $\lesssim 1\%$ (Ferrière 2001; Ferrière 2019). In the regions where neutrals are present, like the WNM and the WIM, the rate of ion-neutral damping depends on the amount and chemical species of the colliding particles. In the WNM and WIM the ions are H^+ , while neutrals are He atoms (with a H/He ratio of $\sim 10\%$) and H atoms with a fraction that varies from phase to phase.

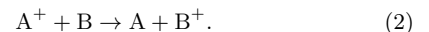
The main processes of momentum transfer (mt) between ions and neutrals are elastic scattering by induced dipole, and charge exchange (ce). In the former case, dominant at low collision energies, the incoming ion is deflected by the dipole electric field induced in the neutral species, according to its polarizability (Langevin scattering); in the latter case the incoming ion takes one or more electrons from the neutral species, which becomes an ambient ion. The friction force per unit volume \mathbf{f}_i exerted on an ion i is thus the sum of $\mathbf{f}_{i,mt} + \mathbf{f}_{i,ce}$.

With the exception of collisions between an ion and a neutral of the same species, as in the important case of collisions of H^+ ions with H atoms (see Sec. A1), the two processes are well separated in energy. At low collision energies elastic scattering dominates, and the friction force is

$$\mathbf{f}_{i,mt} = n_i n_n \mu_{in} \langle \sigma_{mt} v \rangle_{in} (\mathbf{u}_n - \mathbf{u}_i), \quad (1)$$

where n_i and n_n are the ion and neutral densities, \mathbf{u}_i and \mathbf{u}_n are the ion and neutral velocities, μ_{in} is the reduced mass of the colliding particles, σ_{mt} is the momentum transfer (hereafter m.t.) cross section, and the brackets denote an average over the relative velocity of the colliding particles.

At high collision energies (above $\sim 10^2$ eV), the dominant contribution to the transfer of momentum is charge exchange



If the charge exchange rate coefficient is approximately independent of temperature, and there is no net backward-forward asymmetry in the scattering process (two conditions generally well satisfied), Draine (1986) has shown that the friction force on the ions takes the form

$$\mathbf{f}_{i,ce} = n_i n_n \langle \sigma_{ce} v \rangle_{in} \frac{m_n^2 \mathbf{u}_n - m_i^2 \mathbf{u}_i}{m_n + m_i}, \quad (3)$$

where σ_{ce} is the charge exchange (hereafter c.e.) cross section, and m_n (m_i) the mass of the neutral (ion).

The collisional rate coefficients $\langle \sigma_{mt} v \rangle_{in}$ and $\langle \sigma_{ce} v \rangle_{in}$ are often estimated from the values given by Kulsrud & Cesarsky (1971) or Zweibel & Shull (1982) for $H^+ - H$ collisions (e.g. D’Angelo et al. 2016; Nava et al. 2016; Brahimi et al. 2020). The rate coefficients for collisions between various

Table 1. ISM phases and parameters adopted in this work. T is the gas temperature, B the interstellar magnetic field, n the total gas density, f the ionisation fraction, χ the helium fraction and L_{inj} the injection scale of the background magnetic turbulence.

	T (K)	B (G)	n (cm ⁻³)	neutral	ion	f	χ	L_{inj} (pc)
WIM	8000	5	0.35	H, He	H ⁺	0.6 0.9	0 0.1	
				He	H ⁺	1	0.1	50
WNM	8000	5	0.35	H, He	H ⁺	7×10^{-3}	5×10^{-2}	0 0.1 50
CNM	80	5	35	H, He	C ⁺	4×10^{-4}	10^{-3}	0.1 1-50
DiM	50	5	300	H ₂ , He	C ⁺	10^{-4}	0.1	1-50
HIM	10^6	5	~ 0.01	-	H ⁺	1.0	0.0	100

species of ions and neutrals adopted in this study are described in detail in Sec. A1. For elastic collisions, they have been taken from the compilation by Pinto & Galli (2008); for charge exchange, they have been calculated from the most updated available cross sections.

Ion-neutral collisions are one of the dominant damping processes for Alfvén waves propagating in a partially ionized medium (see Piddington 1956; Kulsrud & Pearce 1969). In the case of elastic ion-neutral collisions, (Eq. 1), the dispersion relation for Alfvén waves in this case is

$$\omega(\omega^2 - \omega_k^2) + i\nu_{in}[(1 + \epsilon)\omega^2 - \epsilon\omega_k^2] = 0, \quad (4)$$

where ω is the frequency of the wave, $\omega_k = kv_{A,i}$ is the wavevector in units of the Alfvén speed of the ions

$$v_{A,i} = \frac{B}{\sqrt{4\pi m_i n_i}}, \quad (5)$$

ν_{in} is the ion-neutral collision frequency

$$\nu_{in} = \frac{m_n}{m_i + m_n} \langle \sigma_{\text{mt}} v \rangle_{in} n_n, \quad (6)$$

and ϵ is the ion-to-neutral mass density ratio

$$\epsilon = \frac{m_i n_i}{m_n n_n}. \quad (7)$$

Notice that ϵ is a small quantity in the WNM and CNM but not in the WIM².

The dispersion relation Eq. (4) is a cubic equation for the wave frequency ω (with real and imaginary parts) as a function of the real wavenumber ω_k . Writing $\omega = \Re(\omega) - i \frac{\text{in}}{d}$, where $\frac{\text{in}}{d} > 0$ is the ion-neutral damping rate, and substituting in Eq. (4), one obtains (Zweibel & Shull 1982)

$$\omega_k^2 = \frac{2}{\nu_{in}} \frac{\frac{\text{in}}{d}}{2 - \frac{\text{in}}{d}} [(1 + \epsilon)\nu_{in} - 2 \frac{\text{in}}{d}]^2, \quad (8)$$

which implies $0 < \frac{\text{in}}{d} < \nu_{in}/2$. If $\epsilon \ll 1$, then

$$\frac{\text{in}}{d} \approx \frac{\omega_k^2 \nu_{in}}{2[\omega_k^2 + (1 + \epsilon)^2 \nu_{in}^2]}. \quad (9)$$

Alfvén waves resonantly excited by CR protons have frequency $\omega_k \approx v_{A,i}/r_L$. Thus, the frequency is related to the

² To be precise, the dispersion relation Eq. (4) is valid only if the friction force is proportional to the ion-neutral relative speed v_{in} , as in the case of momentum transfer by elastic collisions. However, we use the same relation also in the case of charge exchange, simply replacing $\langle \sigma_{\text{mt}} v \rangle_{in}$ with $\langle \sigma_{\text{ce}} v \rangle_{in}$.

kinetic energy of the CR proton $E = m_p c^2$ as

$$\omega_k \approx \frac{eBv_{A,i}}{E}. \quad (10)$$

The effective Alfvén velocity, $v_A = \Re(\omega)/k$, felt by CRs depends on the coupling between ions and neutrals. In general, the following asymptotic behavior can be identified:

- Low wavenumber, $\omega_k \ll \nu_{in}$:

at large CR energy ions and neutrals are well coupled; the total density is $n = n_H + n_{\text{He}} + n_i$ and the Alfvén speed relevant for CRs resonant with the waves is

$$v_{A,n} = \frac{B}{\sqrt{4\pi\mu m_p n}}, \quad (11)$$

where $\mu \sim 1.4$ is the mean molecular weight, and $\frac{\text{in}}{d} \propto E^{-2}$;

- High wavenumber, $\omega_k \gg \nu_{in}$:

at small CR energy ions and neutrals are weakly coupled and ion-neutral damping is most effective. The Alfvén speed is the one in the ions, $v_{A,i}$, and $\frac{\text{in}}{d} \sim \text{const.}$

Notice that if $\epsilon < 1/8$ there is a range of wavenumbers for which the waves do not propagate in a partially ionized medium (Zweibel & Shull 1982). This is marked as a shaded region in Fig. 1-2. On the other hand, such non-propagation band is found in the absence of CRs propagating in the partially ionized medium. Recently it has been suggested (Reville et al. 2021) that taking into account the presence of CRs may allow for the propagation of waves in that band.

Introducing the fraction of ionized gas f and the helium-to-hydrogen ratio χ ,

$$f = \frac{n_i}{n_H + n_i}, \quad \chi = \frac{n_{\text{He}}}{n_H + n_i}, \quad (12)$$

Eq. (6) becomes

$$\nu_{in} = \left[\frac{1}{1 + \tilde{m}_i} \langle \sigma_{\text{mt}} v \rangle_{i,H} + \frac{4\chi}{4 + \tilde{m}_i} \langle \sigma_{\text{mt}} v \rangle_{i,\text{He}} \right] \frac{n}{1 + \chi}. \quad (13)$$

where $\tilde{m}_i = m_i/m_p$. In the following, the standard value $\chi = 0.1$ is assumed, but the case $\chi = 0$ is also considered for illustrative purposes and for a comparison with the results of D'Angelo et al. (2016), who neglect the contribution of helium to ion-neutral damping.

2.1.1 WIM and WNM

In this case H is partially ionized and the dominant ion is H⁺ ($\tilde{m}_i = 1$). Therefore $\epsilon = n_H / (n_H + 4n_{\text{He}}) = f/(1 - f + 4\chi)$,

i.e. $\epsilon = 0.005\text{--}0.05$ and $0.75\text{--}9$ for the WNM and the WIM, respectively. The ion-neutral collision frequency is

$$\nu_{in} = \left[\frac{1}{2} f \langle \sigma_{mt} v \rangle_{\text{H}, \text{H}} + \frac{4\chi}{5} \langle \sigma_{mt} v \rangle_{\text{H}, \text{He}} \right] \frac{n}{1+\chi}. \quad (14)$$

Fig. 1 shows the damping rate for waves resonant with CRs of energy E , as a function of the CR energy E . Notice the non-propagation band found in the WNM ($\epsilon < 1/8$).

2.1.2 CNM and DiM

In this case H is neutral and the dominant ion is C^+ ($\tilde{m}_i = 12$), with fractional abundance $n_{\text{C}}/n_{\text{H}} \approx (0.4\text{--}1) \times 10^{-3}$. Therefore $\epsilon = 12n_{\text{C}}/(n_{\text{H}} + 4n_{\text{He}}) \approx (3\text{--}9) \times 10^{-3}$ and

$$\nu_{in} = \left[\frac{1}{13} \langle \sigma_{mt} v \rangle_{\text{C}, \text{H}} + \frac{\chi}{4} \langle \sigma_{mt} v \rangle_{\text{C}, \text{He}} \right] \frac{n}{1+\chi}. \quad (15)$$

Fig. 2 shows the damping rate for waves resonant with CRs of energy E , as a function of the CR energy E . Also in this case non-propagation regions are found.

2.2 Wave cascade and turbulent damping

The turbulent damping (FG) of self-generated Alfvén waves is due to their interaction with a pre-existing background turbulence. Such turbulence may be injected by astrophysical sources (see e.g. Mac Low & Klessen 2004) with a turbulent velocity v_{turb} and on scales, L_{inj} , much larger than the CR Larmor radius. For waves in resonance with particles with a given energy E , the damping rate, that accounts for the anisotropy of the turbulent cascade, has been derived by Farmer & Goldreich (2004); Yan & Lazarian (2004) and reads

$$\frac{\text{FG}}{d} = \left(\frac{v_{\text{turb}}^3 / L_{\text{inj}}}{r_{\text{L}} v_{\text{A}}} \right)^{1/2}, \quad (16)$$

where v_{A} is the effective Alfvén speed felt by CRs, as defined in Sec. 2.1. We take the turbulence as trans-Alfvénic at the injection scale, namely $v_{\text{turb}} = v_{\text{A},n}$ (at large scales waves are in the low wavenumber regime, where ions and neutrals are well coupled, as illustrated in Sec. 2.1). This is the likely situation if the turbulence is mainly injected by old SNRs, with a forward shock becoming trans-sonic and trans-Alfvénic. The FG damping rate is shown in Fig. 1 for the WIM and WNM.

In highly neutral media, such as the the WNM, CNM and DiM, the background turbulence responsible for the FG damping can be damped by ion-neutral friction at a scale, $l_{\text{min}} = 1/k_{\text{min}}$ (Xu et al. 2015, 2016; Lazarian 2016; Brahimi et al. 2020). Correspondingly, there is a minimum particle energy, E_{min} , such that $r_{\text{L}}(E_{\text{min}}) = l_{\text{min}}$, below which the FG damping cannot affect the self-generated Alfvén waves (Brahimi et al. 2020):

$$\frac{1}{l_{\text{min}}} = L_{\text{inj}}^{1/2} \left(\frac{2\epsilon\nu_{in}}{v_{\text{A},n}} \right)^{3/2} \sqrt{1 + \frac{v_{\text{A},n}}{2\epsilon\nu_{in}L_{\text{inj}}}}. \quad (17)$$

In Fig. 1 the FG damping rate for the WNM is truncated at E_{min} . In the WIM the cascade rate is found to be always larger than the ion-neutral damping rate and there is no E_{min} .

2.3 Non-linear Landau damping

The non-linear Landau (NLL) damping is caused by the interaction between the beat of two Alfvén waves and the thermal (at temperature T) ions in the background medium. The damping rate for resonant waves is given by (Kulsrud 1978; Wiener et al. 2013)

$$\frac{\text{NLL}}{d} = \frac{1}{2} \sqrt{\frac{\pi}{2}} \left(\frac{k_{\text{B}} T}{m_{\text{p}}} \right) \frac{I(k_{\text{res}})}{r_{\text{L}}}, \quad (18)$$

where k_{B} is the Boltzmann constant and $I(k_{\text{res}})$ is the wave energy density (see Sec. 3 below for the definition) at the resonant wavenumber $k_{\text{res}} = 1/r_{\text{L}}$.

3 COSMIC RAY PROPAGATION IN THE PROXIMITY OF SNRS

We consider the escape of CRs from a SNR and the subsequent propagation in the source proximity. The propagation region is assumed to be embedded in a turbulent magnetic field, with a large scale ordered component of strength B_0 . CRs are scattered by Alfvén waves, which constitute a turbulent magnetic field background of relative amplitude $\delta B/B_0$, where k is the wavenumber. We only consider waves that propagate along the uniform background field B_0 . In the limit of $\delta B/B_0 \ll 1$, which is the one relevant for the cases treated in this paper, the CR diffusion along field lines can be treated in the quasi-linear regime, with a diffusion coefficient given by Berezhinskii et al. (1990) and Kulsrud (2005)

$$D(E) = \frac{4\pi c r_{\text{L}}(E)}{3I(k_{\text{res}})} \Big|_{k_{\text{res}}=1/r_{\text{L}}} = \frac{D_{\text{B}}(E)}{I(k_{\text{res}})}, \quad (19)$$

where c is the speed of light, $I(k_{\text{res}}) = \delta B(k_{\text{res}})^2/B_0^2$ is the wave energy density calculated at the resonant wavenumber $k_{\text{res}} = 1/r_{\text{L}}$, and $D_{\text{B}}(E) = (4\pi/3)cr_{\text{L}}(E)$ is the Bohm diffusion coefficient. We also assume that the dominant source of Alfvénic turbulence is produced by the CR resonant streaming instability.

In our model we adopt the flux tube approximation for the CR transport along B_0 (see, e.g., Ptuskin et al. 2008), and we neglect the diffusion across field lines, which is suppressed in the $\delta B/B_0 \ll 1$ regime (see e.g. Drury 1983; Casse et al. 2002). Thus, we do not address the perpendicular evolution of the flux tube (see, e.g., Nava & Gabici 2013) and any possible CR feedback on it and, in general, on the ISM dynamics (see, e.g., Schroer et al. 2020). Such one-dimensional model for the CR propagation is applicable for distances from the source below the coherence length, L_c , of the background magnetic turbulence, i.e. the scale below which the magnetic flux tube is roughly preserved (see, e.g., Casse et al. 2002).

When particles diffuse away from the source at distances larger than L_c , diffusion becomes 3-D and the CR density drops quickly. In the Galactic disk, L_c is estimated observationally and may range from few pc to ≈ 100 pc, depending on the ISM phase (see, e.g., Nava & Gabici 2013, and references therein).

We follow the approach proposed by Nava et al. (2016, 2019), and we determine: (i) the escape time of CRs of a

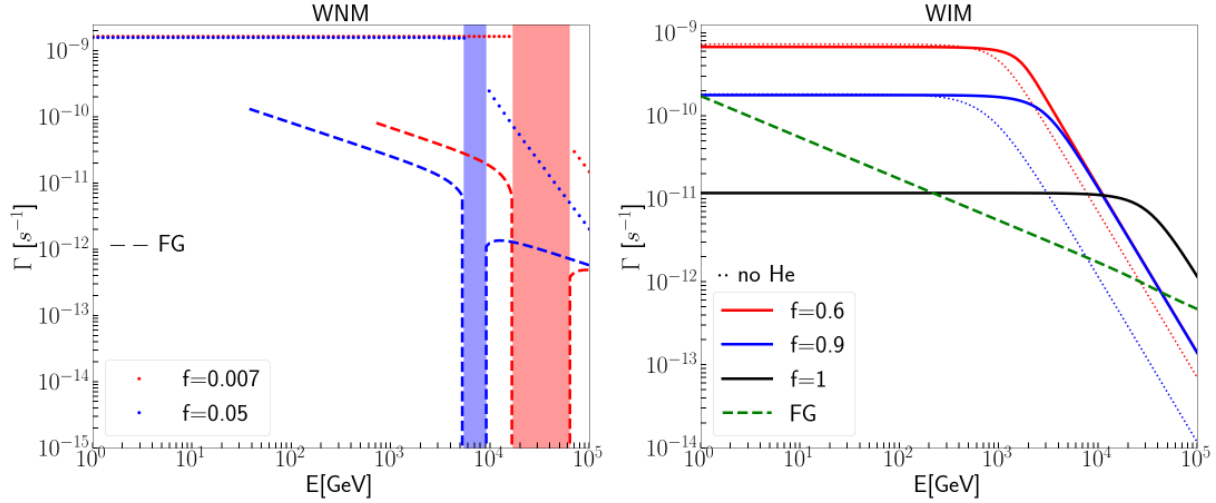


Figure 1. Damping rates Γ_d^{in} and Γ_d^{FG} (ion-neutral and turbulent) of Alfvén waves in the WNM (left-hand panel) and WIM (right-hand panel) vs. CR energy E . Different colors are used for different values of the hydrogen ionization fraction f . Unless stated otherwise, a standard $\chi = 0.1$ He abundance is assumed. The considered parameters for the WNM and WIM are given in Table 1. In the left-hand panel the dotted lines refer to ion-neutral damping, while the dashed lines to the FG damping. The last are truncated to the minimum energy, E_{\min} , below which the background turbulence is damped by ion-neutral friction before reaching the scale relevant for damping self-generated waves resonant with particle of energy $< E_{\min}$ (see Sec. 2.2). The shaded regions represent the range of non-propagation of Alfvén waves (see Sec. 2.1). In the right-hand panel, the solid lines refer to ion-neutral damping, while the thin dotted lines refer to the case where the contribution to damping from He is neglected ($\chi = 0$). The dashed lines refer to the FG damping, which in the case of WIM is found to depend little on the ionization fraction f .

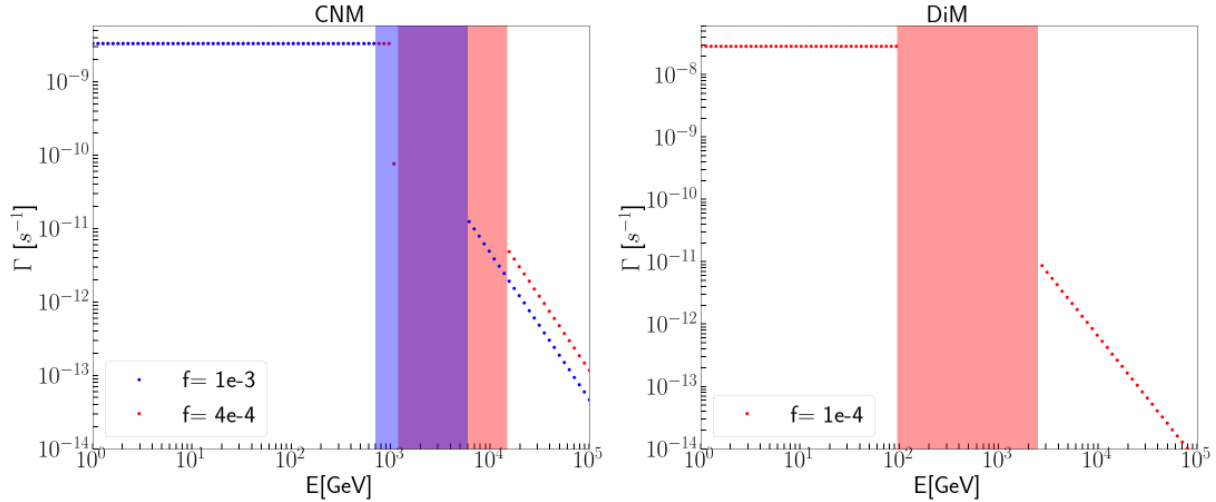


Figure 2. Ion-neutral damping rate Γ_d^{in} of Alfvén waves in the CNM (left-hand panel) and DiM (right-hand panel) as a function of the CR energy E . Different colors are used for different values of the C^+ abundance. The parameters adopted for the CNM and DiM are given in Table 1. The shaded regions represent the range of non-propagation of Alfvén waves (see Sec. 2.1).

given energy from the remnant; (ii) the time dependent evolution of the CR cloud and of the self-generated diffusion coefficient after escape; (iii) the time spent by CRs in the source vicinity and the corresponding grammage. We focus on the warm ionized and warm neutral phases of the ISM. As shown in the following sections, the results depend significantly on the considered ISM phase, and in particular on the amount and type of neutral and ionized atoms in the background medium.

3.1 Transport equations and initial/boundary conditions

The coupled CR and wave transport equations read (Nava et al. 2016, 2019)

$$\frac{\partial P_{\text{CR}}}{\partial t} + v_A \frac{\partial P_{\text{CR}}}{\partial z} = \frac{\partial}{\partial z} \left(\frac{D_B}{I} \frac{\partial P_{\text{CR}}}{\partial z} \right) \quad (20)$$

and

$$\frac{\partial I}{\partial t} + v_A \frac{\partial I}{\partial z} = 2(\text{CR } a)I + Q. \quad (21)$$

Here v_A is an effective Alfvén velocity that takes into account the coupling between ions and neutrals (see Sec. 2.1), while P_{CR} is the partial pressure of CRs of momentum p normalized to the magnetic field pressure

$$P_{\text{CR}} = \frac{4\pi}{3} c p^4 \frac{f(p)}{B_0^2/8\pi}. \quad (22)$$

The term $2_{\text{CR}}I$ gives the wave growth due to the CR streaming instability and can be expressed as

$$2_{\text{CR}}I = v_A \frac{\partial P_{\text{CR}}}{\partial z}. \quad (23)$$

The term $_{\text{d}}$ encompasses the relevant wave damping rates, which are described in detail in Sec. 2. The term Q represents the possible injection of turbulence from an external source, other than the CR streaming. Here it is taken as $Q = 2_{\text{d}}I_0$, where I_0 is a parameter such that typical values of the Galactic CR diffusion coefficient are recovered at large distances from the source (see, e.g., Strong et al. 2007). In this way, when the streaming instability is not relevant, diffusion is regulated by the background turbulence. Notice that in these equations we neglected adiabatic losses that arises when Alfvén speed varies in space (see, e.g., Brahimi et al. 2020), since we are considering a homogeneous ISM around the SNR.

The coordinate z is taken along B_0 and $z = 0$ refers to the centre of the CR source. The equations are solved numerically with a finite difference explicit method, using the initial conditions

$$P_{\text{CR}} = \begin{cases} P_{\text{CR}}^0 & \text{if } z < R_{\text{esc}}(E), \\ 0 & \text{if } z > R_{\text{esc}}(E), \end{cases}$$

and

$$I = I_0 \quad \text{everywhere.} \quad (24)$$

Here $R_{\text{esc}}(E)$ is the size of the region filled by CRs at the time of escape, and P_{CR}^0 is the initial CR pressure inside this region. The method used to determine the escape radius and time for particles of energy E is described in detail in Nava et al. (2016, 2019). As for the initial condition for the waves, it is also possible to choose $I \gg I_0$ for $z < R_{\text{esc}}(E)$ in order to mimic Bohm diffusion inside the source, as proposed by Malkov et al. (2013). However, as discussed by Nava et al. (2019), different choices of I inside the source have little impact on the final solution. As boundary conditions we impose a symmetric CR distribution at $z = 0$, and

$$P_{\text{CR}} = 0, \quad I = I_0 \quad \text{at } z = L_c. \quad (25)$$

The 1-D model used in this paper is valid only up to a distance from the source given by the coherence length L_c of the magnetic field. At larger distances the diffusion becomes 3-D and the CR density quickly drops, a behavior that can be described in terms of a free escape boundary at L_c . The value of L_c is constrained from observations to be $\lesssim 100$ pc but its value is matter of debate and is likely phase- and position-dependent in our galaxy. We take the free escape boundary at $z = L_c$, and we check that this assumption is not significantly affecting the results, for instance changing L_c to $10 L_c$.

4 RESULTS

In what follows we discuss the release of CRs of energy E from a SNR, giving an estimate of the age and radius of the source at the moment of escape. Moreover, we investigate the propagation of runaway CRs in the source proximity, with particular focus on the CR spectrum and self-generated diffusion coefficient. Finally, we estimate the residence time of CRs in the source proximity and we infer general implications for the grammage accumulated in that region.

We treat these aspects in the cases of a WIM or a WNM surrounding the remnant, with special emphasis on the role played by the ion-neutral damping of Alfvén waves.

In our calculations we assume that: (i) runaway CRs have a total energy $E_{\text{CR}} = 10^{50}$ erg, a power-law spectrum in energy between 1 GeV–5 PeV with spectral index $\gamma = 2.0$; and (ii) the typical ISM diffusion coefficient is $D(E) = D_0(E/10 \text{ GeV})^{0.5}$ with $D_0 = 10^{28} \text{ cm}^2 \text{ s}^{-1}$ (see, e.g., Strong et al. 2007).

4.1 Escape of cosmic rays: source age and radius

The age and radius of escape of CRs of energy E is estimated as follows (Nava et al. 2016, 2019): we define the half-time, $t_{1/2}(E, R)$ of a CR cloud as the time after which half of the CRs of a given energy, initially confined within a region of size R , have escaped that region. The evolution of such CR cloud is studied by solving Eq. (20) and Eq. (21) with initial conditions given by Eq. (24) and boundary conditions given by Eq. (25).

The radius of a SNR expanding in a homogeneous medium of density n can be estimated as (Truelove & McKee 1999)

$$R_{\text{SNR}}(t) = 0.5 \left(\frac{E_{51}}{n} \right)^{1/5} \left[1 - \frac{0.09 M_{\text{ej}\odot}^{5/6}}{E_{51}^{1/2} n^{1/3} t_{\text{kyr}}} \right]^{2/5} t_{\text{kyr}}^{2/5} \text{ pc}, \quad (26)$$

where E_{51} is the supernova explosion energy in units of 10^{51} erg, n is the total density of the ambient ISM in cm^{-3} , $M_{\text{ej}\odot}$ is the mass of the supernova ejecta in solar masses, and t_{kyr} is the SNR age in kyr. This equation is valid in the adiabatic phase of the expansion, which starts after $\approx 86 M_{\text{ej}\odot}^{5/6} E_{51}^{1/2} n^{-1/3}$ yr. Here we take $E_{51} = 1$ and $M_{\text{ej}\odot} = 1.4$, while the gas density depends on the medium and is reported in Table 1. At earlier times an approximate expression for the free expansion phase has to be used (Chevalier 1982). The adiabatic phase stops at roughly $\approx 1.4 \times 10^4 E_{51}^{3/14} n^{-4/7}$ yr, when the radiative phase starts (Cioffi et al. 1988). At this epoch we also assume that the acceleration of CRs becomes ineffective and that all CRs are instantly released (the validity of the assumption of instant release may depend on the conditions in the shock precursor, as discussed by Brahimi et al. 2020).

The escape time, $t_{\text{esc}}(E)$, of particles with energy E is estimated as the time such that $t_{1/2}(E, R_{\text{SNR}})$ equals the age of a SNR of radius R_{SNR} . This is the timescale over which waves can grow. The dependence of $t_{1/2}(E, R)$ on the initial radius R at fixed energy E , and varying the background diffusion coefficient and the CR spectral index, has been extensively explored by Nava et al. (2016, 2019), and we refer the reader to these works for a detailed discussion. Here we briefly summarize the most relevant points. At small

R the CR gradient is large and the amplification of waves is very effective. In this regime, the NLL damping, that scales with the wave energy density $I(k)$, can play an important role and may dominate over ion-neutral and FG damping at small enough radii. At intermediate R , ion-neutral damping dominates in most cases. In fact, as shown in Fig. 1, the ion-neutral damping rate is larger than the FG rate at least up to particle energies of ~ 10 TeV, with the only exception of a WIM with fully ionized hydrogen and $\sim 10\%$ of neutral helium. At large R , the CR gradient is reduced and the streaming instability is less effective. In this case the expansion of the CR bubble is determined by the background turbulence and the test particle limit is recovered, with $t_{1/2} \propto R^2/D_0$.

Fig. 3 and Fig. 4 show the SNR age and radius at the time of escape of CRs, as a function of the CR energy, in the case of a WNM and WIM respectively. We confirm the findings by Nava et al. (2016, 2019) and the qualitative results that particles with higher energy escape earlier than the low energy particles (see, e.g., Gabici 2011).

In the case of the WIM, R_{esc} and t_{esc} tend to decrease with a larger neutral density. The effect of ion-neutral damping is especially visible in the energy range ~ 1 –10 TeV, where the ion-neutral damping rate starts to decrease from a roughly constant value at different particle energies, depending on the value of the ionized hydrogen fraction f and on the helium-to-hydrogen ratio χ , as shown in Fig. 1. The drop of $\frac{in}{d}$ corresponds to an increase of t_{esc} , and therefore to a better CR confinement.

The situation is more subtle in the case of the WNM. In fact, here the confinement appears to be slightly more effective for a smaller value of f , a result opposite to what happens in the WIM. This can be explained taking into account that, while the $\frac{in}{d}$ is practically the same at energies below ~ 10 TeV for $f \sim 7 \times 10^{-3}$ – 5×10^{-2} , the effective Alfvén speed felt by CRs, which at these energies is roughly that of ions, as illustrated in Sec. 2, is a factor of ~ 2 –3 larger for $f = 7 \times 10^{-3}$. This reflects on an increase by the same amount of the FG damping rate (above the cut-off energy, see Sec. 2.2), as shown in Fig. 1, but also of the growth rate term, which is proportional to v_A . On the other hand, at energies in the range ~ 10 GeV–1 TeV, the FG damping is always subdominant compared to the ion-neutral damping, and the net effect of this change of v_A is a slightly better confinement at smaller f as a result of an enhanced wave growth rate.

Also in the case of a WIM the effective v_A is a bit larger at smaller f below ~ 1 TeV, but here the increase is only by a factor of ~ 1.2 and cannot overcome the effect of ion-neutral damping.

4.2 Cosmic ray spectra and diffusion coefficient

The spectrum of runaway CRs and the corresponding self-generated turbulence depend significantly on the distance from the source and on the time. In Fig. 5 and Fig. 6 we show the spectrum of CRs that have already escaped to a distance of 50 pc from the centre of the remnant at different times, from $t = 6 \times 10^3$ yr to $t = 10^5$ yr, and for the WNM ($f = 0.05$, $\chi = 0.1$) and the WIM ($f = 0.9$, $\chi = 0.1$), respectively. To remove the effect of the simple 1-D geometry that we are adopting we multiply P_{CR} by $R_{\text{esc}}^2(E)/R_{\text{SNR}}^2(t)$. For each

case we also show the ratio between the self-generated and background diffusion coefficients.

In the same figures we also show the spectrum and diffusion coefficient at the position of the shock of CRs that have escaped at earlier times (and are considered as decoupled from the accelerator) as well as the spectrum of particle still confined in the accelerator, at different ages of the remnant from $t = 6 \times 10^3$ yr to $t = 3 \times 10^4$ yr. The spectrum of the confined particles is estimated by assuming that the remnant provides $\approx 10^{50}$ erg in CRs with a $\propto E^{-2}$ spectrum that extends from ~ 1 GeV to ~ 5 PeV, with an exponential cutoff at the energy of the particles that escape at the considered age. The SNR is assumed to stop accelerating particles at the onset of the radiative phase, which for the typical density of the WIM and WNM takes place at $t_{\text{rad}} \approx 3 \times 10^4$ yr. The corresponding shock radius is $R_{\text{rad}} \approx 22$ pc. In all cases, at each time and location, the spectrum exhibit a sharp rise at low energies and a peak followed by a nearly power-law like behaviour at higher energies.

Since high energy particles escape earlier and diffuse faster, they reach a given distance at earlier times, as shown for the spectra at 50 pc, where the peak moves at lower energies with time. At energies lower than the peak, particles have not yet reached that position, giving the sharp rise. At larger energies, particles have diffused over a bigger distance, giving a spectrum steeper than the spectrum released from the SNR, here assumed to be $\propto E^{-2}$.

A similar behaviour is observed with the spectra at the shock. Here the position at which the spectra are shown varies with time, since it is given by the shock radius at a given age. This radius is always < 50 pc for the cases illustrated here. Comparing the spectra at the shock and at 50 pc for a given age, it is evident that the peak is at lower energy in the former case. This again is the result of an earlier escape and faster diffusion of high energy particles.

As for the D/D_0 ratio as a function of energy, it is possible to infer from the plots that, at a given time, the diffusion coefficient is equal to its background value at low energies, where particles have not yet escaped or not yet reached the position where D is calculated, and at high energies, where the turbulence produced by such particle is being damped. At intermediate energies, and roughly corresponding to the peak in the spectrum, the diffusion coefficient is suppressed compared to D_0 due to CR streaming instability. The energies at which the suppression is evident move to lower values with time.

A more complex situation can be observed in some cases, for instance at $t = 10^4$ yr at the shock and in the TeV range, for the WIM. Here D starts to deviate from D_0 at ~ 50 GeV, then, above ~ 500 GeV, D begins to approach again D_0 , but above ~ 3 TeV the level of turbulence increases again, with the result of a suppression of D . This is due to the energy dependence of the escape radius, which becomes steeper above few TeV. This results in the fact that, above that energy, the escape radius becomes small enough as to effectively excite the streaming instability. In fact the density of runaway CRs is $\propto 1/R_{\text{esc}}^2$. The more efficient self-confinement at this high energies also reflects in a hardening of the spectrum (see also Nava et al. 2019 for a discussion).

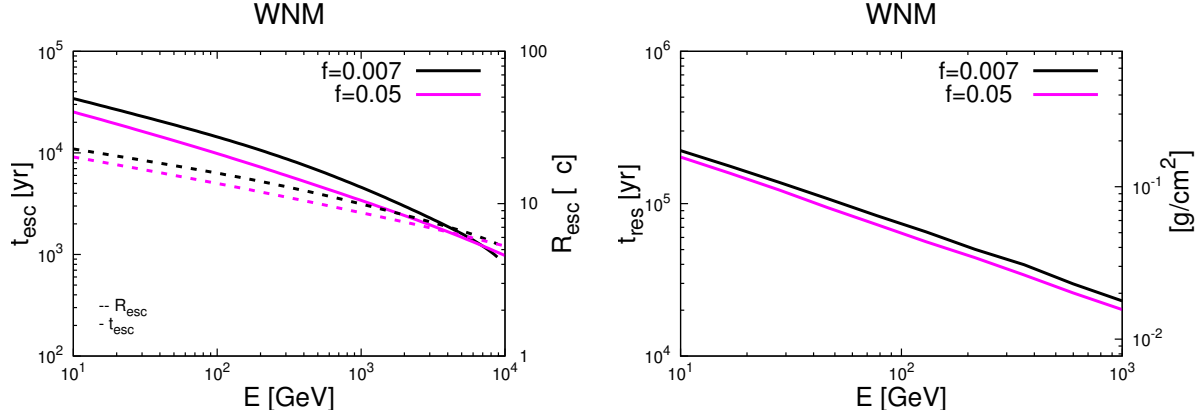


Figure 3. Case of WNM. *Left panel:* SNR age and radius at the time of escape of CRs, as a function of the CR energy. *Right panel:* Residence time of CRs in a region of ~ 100 pc around the source, as a function of the CR energy, and the corresponding grammage. Different colors are used for different values of the hydrogen ionization fraction f , while the helium-to-hydrogen ratio $\chi = 0.1$. The parameters of the WNM are listed in Table 1.

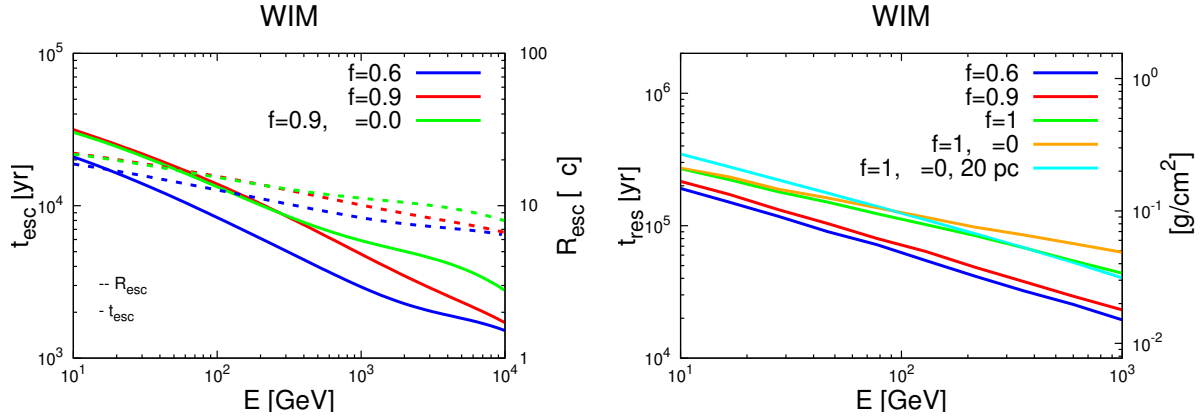


Figure 4. Case of WIM. *Left panel:* SNR age and radius at the time of escape of CRs, as a function of the CR energy. *Right panel:* Residence time of CRs in a region of ~ 100 pc around the source, as a function of the CR energy, and the corresponding grammage. The cyan curve is computed by assuming that particles of all energies escape at SNR radius of 20 pc, as assumed by D’Angelo et al. (2016). Different colors are used for different values of the hydrogen ionization fraction f and helium-to-hydrogen ratio χ . The parameters of the WIM are listed in Table 1.

4.3 Residence time and grammage

The grammage accumulated by CRs close to their sources, and its relevance compared to the grammage accumulated while diffusing in the whole Galaxy, is related to the residence time in the proximity of the source. A formal determination of the grammage should be done by solving the CR transport equation for nuclei with the inclusion of spallation contributions (see, e.g., Berezhinskii et al. 1990; Ptuskin & Soutoul 1990).

Here we adopt the following approach: we assume that N_0 particles of energy E are instantly injected by a source located in a region of constant gas density $\rho = \mu m_p n$ and are subject to free escape at a boundary located at a distance L_c from the source. At a given time t , the total number of particles that are still in the region is $N_{\text{in}}(t)$ while the number of escaped particles is $N_{\text{esc}} = N_0 - N_{\text{in}}(t)$. Particles that cross the boundary at time t have accumulated the grammage $X(t) = \rho c t$ and the average grammage gained by

all escaped particles from $t = 0$ to $t = \infty$ is given by

$$\begin{aligned} \langle X \rangle &= \frac{1}{N_0} \int_0^\infty \rho c t \frac{dN_{\text{esc}}}{dt} dt \\ &= \frac{\rho c}{N_0} \left[\int_0^\infty N_{\text{in}}(t) dt - \lim_{t \rightarrow \infty} (t N_{\text{in}}(t)) \right] \\ &= \rho c \tau_{\text{res}}. \end{aligned} \quad (27)$$

The residence time τ_{res} is given by

$$\tau_{\text{res}} = \frac{1}{N_0} \left[\int_0^\infty N_{\text{in}}(t) dt - \lim_{t \rightarrow \infty} (t N_{\text{in}}(t)) \right]. \quad (28)$$

The number of particles with a given energy contained in the region at a given time can be calculated from the CR pressure (see Sec. 3):

$$N_{\text{in}}(t) = \frac{N_0}{R_{\text{esc}} P_{\text{CR}}^0} \int_0^{L_c} P_{\text{CR}}(z, t, E) dz, \quad (29)$$

where we took into account that CRs on energy E are initially released from a region of size $R_{\text{esc}}(E)$.

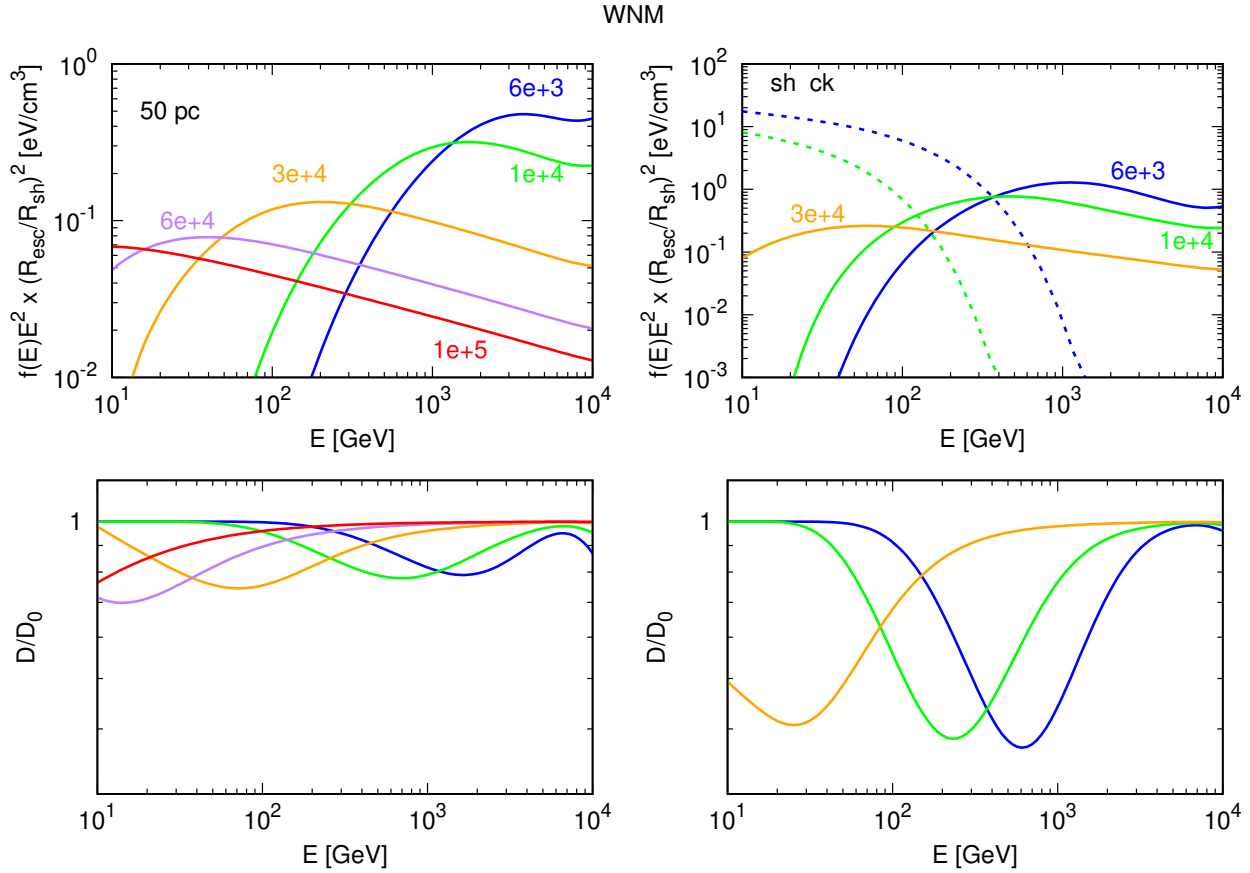


Figure 5. Case of WNM ($f = 0.05$, $\chi = 0.1$): CR spectrum and ratio D/D_0 as a function of energy, where $D_0(E) = 10^{28}(E/10\text{ GeV})^{0.5}\text{ cm}^2\text{ s}^{-1}$. The different colors refer to different ages in yr (as marked). The left panels refer to a location at 50 pc from the center of the SNR, while the right panels refer to the shock position. In this case also the spectrum of CRs still confined in the accelerator is shown (dashed lines).

Fig. 3 and 4 show the residence time of CRs in a region of ~ 100 pc around the remnant, for the WNM and the WIM, respectively, and for different values of the neutral fraction, and the corresponding grammage. Even in the (not very plausible) case of a fully ionized WIM ($f = 1.0$, $\chi = 0.0$), the grammage is nearly two orders of magnitude smaller than that accumulated in the disk (see e.g. Jones et al. 2001; Gabici et al. 2019). This is due to the action of the ion-neutral and FG damping. The presence of a $\sim 10\%$ of neutral helium (which is less effective at wave damping compared to hydrogen) noticeably reduces the CR residence time compared to the case of a fully ionized background medium, above few tens GeV.

These results are at odds with what previously suggested by D’Angelo et al. (2016), namely that ion-neutral damping is totally negligible in the case of only neutral helium, since the c.e. cross section is very small. However, as shown in Sec. 2, not only c.e. but also m.t. has to be taken into account in the ion-neutral damping. In fact, D’Angelo et al. (2016) find a grammage nearly a factor of ten larger than what we find. This is in part due to their assumption of ion-neutral damping of waves with neutral helium. In ad-

dition, they assume a 20% acceleration efficiency, while we assume 10%, which enhances the effect of streaming instability, and they do not include the FG damping. Finally, D’Angelo et al. (2016) assume that CRs at all energies are released when the SNR radius is 20 pc, a scenario implying a smaller release radius at low energies compared to our calculation, which translates in an enhancement of the streaming instability (and the CR confinement) at energies below ≈ 1 TeV, as shown in Fig. 4.

Any addition of neutral hydrogen compared to the case of only neutral helium further reduces the confinement time. Correspondingly, the CR grammage accumulated in the source proximity results to be well below that inferred from observations. A similar result was found by Nava et al. (2019) for the HIM, where the residence time tends to be larger than in a partially ionized medium, but the ISM density is lower ($\sim 0.01\text{ cm}^{-3}$).

5 CONCLUSIONS

We followed the method and the setup proposed by Nava et al. (2016, 2019) to investigate the escape of CRs from

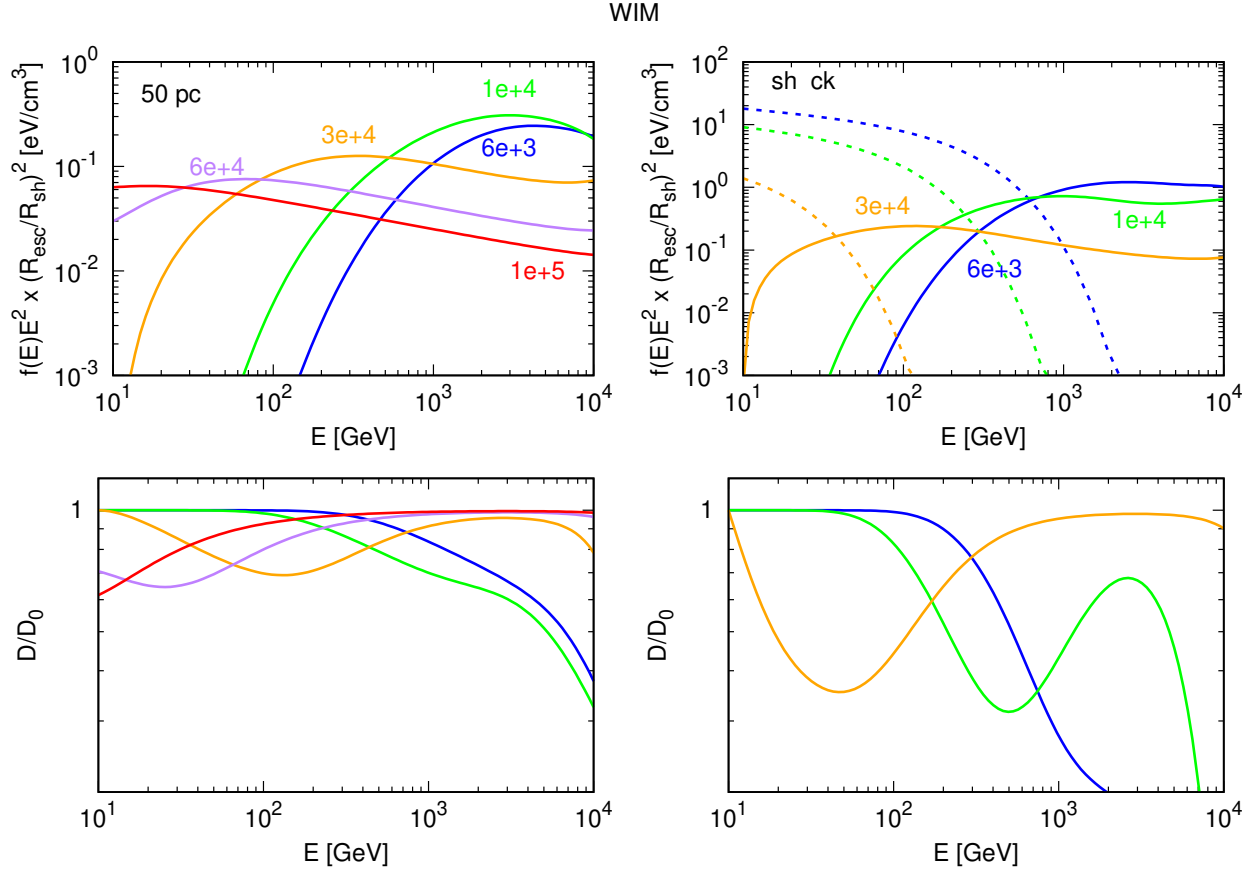


Figure 6. Case of WIM ($f = 0.9$, $\chi = 0.1$): CR spectrum and ratio D/D_0 as a function of energy, where $D_0(E) = 10^{28}(E/10 \text{ GeV})^{0.5} \text{ cm}^2 \text{ s}^{-1}$. The different colors refer to different ages in yr (as marked). The left panels refer to a location at 50 pc from the center of the SNR, while the right panels refer to the shock position. In this case also the spectrum of CRs still confined in the accelerator is shown (dashed lines).

SNRs embedded in a WNM and WIM, and the CR self confinement in the source proximity. Our main objective was to determine whether, in realistic situations, the grammage accumulated by CRs in the source region could become comparable to that inferred from observations. ~~If this was the case,~~ In this case, the standard picture in which CR secondaries are produced during the whole time spent by cosmic rays throughout the disk of the Galaxy, should be profoundly revisited.

We confirm the results found by [Nava et al. \(2016, 2019\)](#) that CRs escaping from SNRs drive the excitation of Alfvén waves through the resonant CR streaming instability, which results in a suppression of the diffusion coefficient and in the CR self-confinement in the source region. The SNR radius at which CRs of a given energy leave the source, $R_{\text{esc}}(E)$, results to be a decreasing function of the energy, and regulates the CR streaming instability through a dilution factor $\propto 1/R_{\text{esc}}^2$.

We found that the growth of self-generated Alfvén waves, and consequently the residence time of CRs in the source region, is significantly limited by several damping processes, especially by the FG and ion-neutral damping.

In particular, for the ion-neutral damping of Alfvén waves we have used up-to-date damping coefficients, based on accurate experimental or theoretical determinations of the momentum transfer and charge exchange cross sections between ions and neutrals of different species.

In the 1-D geometry adopted in our calculation a suppression of the diffusion coefficient is found within a distance from the source of the order of the magnetic field coherence length $L_c \approx 50 - 100 \text{ pc}$, for a timescale that can be as large as $\sim 10^5 \text{ yr}$ at $\sim 10 \text{ GeV}$. A smaller value for L_c would make the CR propagation to become 3-D closer to the remnant, thus reducing the residence time compared to our results.

We conclude that ion-neutral damping strongly limits the CR grammage that can be accumulated in the source region. Under the conditions typically met in the WIM and WNM of the Galactic disk, the CR source grammage is found to be negligible compared to that inferred from observation. A similar result was found for the HIM by [Nava et al. \(2019\)](#), where the CR residence time is typically larger than in a partially ionized medium but the ISM density is more than a factor ten smaller. This makes alternative scenarios for the interpretation of quantities such as the B/C

ratio, in which an important contribution to the production of secondaries comes from the source region, less attractive.

Our results on the residence time (and grammage) may change with the inclusion of the contribution of other sources of turbulence to the CR confinement. In particular, it has recently been suggested that ~~an other~~ another CR-induced instability, the so called *non resonant streaming instability*, which is mediated by the CR current and plays a crucial role in the acceleration of CRs (Bell 2004), may significantly enhance the CR self-confinement in the source region above \sim TeV energies (Schroer et al. 2020). Further investigations are thus needed in order to firmly establish the ~~importance~~ amount of CR grammage accumulated in the vicinity of sources by very-high energy particles.

REFERENCES

- Aharonian F. A., Atoyan A. M., 1996, *A&A*, **309**, 917
 Amato E., 2011, *Mem. Soc. Astr. It.*, **82**, 806
 Bell A. R., 2004, *Monthly Notices of the Royal Astronomical Society*, **353**, 550
 Berezhinskii V. S., Bulanov S. V., Dogiel V. A., Ptuskin V. S., 1990, *Astrophysics of Cosmic Rays*
 Blasi P., 2013, *A&ARv*, **21**, 70
 Brahim L., Marcowith A., Ptuskin V. S., 2020, *A&A*, **633**, A72
 Brennan M. H., Morrow R., 1971, *J. Phys. B*, **4**, L53
 Casanova S., et al., 2010, *PASJ*, **62**, 1127
 Casse F., Lemoine M., Pelletier G., 2002, *Phys. Rev. D*, **65**, 023002
 Cesarsky C. J., 1980, *ARA&A*, **18**, 289
 Chevalier R. A., 1982, *ApJ*, **258**, 790
 Cho J., Lazarian A., 2002, *Phys. Rev. Lett.*, **88**, 245001
 Cioffi D. F., McKee C. F., Bertschinger E., 1988, *ApJ*, **334**, 252
 D’Angelo M., Blasi P., Amato E., 2016, *Phys. Rev. D*, **94**, 083003
 Dalgarno A., 1958, *Phil. Trans. Roy. Soc. Lon. A*, **250**, 426
 Draine B. T., 1986, *MNRAS*, **220**, 133
 Drury L. O., 1983, *Rep. Progr. Phys.*, **46**, 973
 Farmer A. J., Goldreich P., 2004, *ApJ*, **604**, 671
 Felice G. M., Kulsrud R. M., 2001, *ApJ*, **553**, 198
 Ferrière K. M., 2001, *Rev. Mod. Phys.*, **73**, 1031
 Ferrière K., 2019, *Plasma Physics and Controlled Fusion*, **62**, 014014
 Flower D. R., Pineau des Forets G., 1995, *MNRAS*, **275**, 1049
 Fornieri O., Gaggero D., Cerri S. S., De La Torre Luque P., Gabici S., 2021, *MNRAS*, **502**, 5821
 Gabici S., 2011, *Mem. Soc. Astron. Italiana*, **82**, 760
 Gabici S., Aharonian F. A., Casanova S., 2009, *MNRAS*, **396**, 1629
 Gabici S., Evoli C., Gaggero D., Lipari P., Mertsch P., Orlando E., Strong A., Vittino A., 2019, *Int. J. Mod. Phys. D*, **28**, 1930022
 Glassgold A. E., Krstić P. S., Schultz D. R., 2005, *ApJ*, **621**, 808
 Goffe T. V., Shah M. B., Gilbody H. B., 1979, *J. Phys. B*, **12**, 3763
 Hodges R. R., Breig E. L., 1991, *J. Geophys. Res.*, **96**, 7697
 Jean P., Gillard W., Marcowith A., Ferrière K., 2009, *A&A*, **508**, 1099
 Jones F. C., Lukasiak A., Ptuskin V., Webber W., 2001, *ApJ*, **547**, 264
 Krstić P. S., Schultz D. R., 1999, *J. Phys. B*, **32**, 3485
 Krstić P. S., Schultz D. R., 2006, *Phys. Plasmas*, **13**, 053501
 Kulsrud R. M., 1978, in Reiz A., Andersen T., eds, *Astronomical Papers Dedicated to Bengt Stromgren*. pp 317–326
 Kulsrud R. M., 2005, *Plasma Physics for Astrophysics*
 Kulsrud R. M., Cesarsky C. J., 1971, *Astrophys. Lett.*, **8**, 189
 Kulsrud R., Pearce W. P., 1969, *ApJ*, **156**, 445
 Kusakabe T., Sakaue H. A., Tawara H., 2011, *Plasma Fus. Res.*, **6**, 2401102
 Lazarian A., 2016, *ApJ*, **833**, 131
 Loreau J., Ryabchenko S., Burgos J. M. M., Vaeck N., 2018, *J. Phys. B*, **51**, 085205
 Mac Low M.-M., Klessen R. S., 2004, *Rev. Mod. Phys.*, **76**, 125
 Malkov M. A., Diamond P. H., Sagdeev R. Z., Aharonian F. A., Moskalenko I. V., 2013, *ApJ*, **768**, 73
 Martin P. J., et al., 1981, *Phys. Rev. A*, **23**, 2858
 Nava L., Gabici S., 2013, *MNRAS*, **429**, 1643
 Nava L., Gabici S., Marcowith A., Morlino G., Ptuskin V. S., 2016, *MNRAS*, **461**, 3552
 Nava L., Recchia S., Gabici S., Marcowith A., Brahim L., Ptuskin V., 2019, *MNRAS*, **484**, 2684
 Newman J. H., Cogan J. D., Ziegler D. L., Nitz D. E., Rundel R. D., Smith K. A., Stebbings R. F., 1982, *Phys. Rev. A*, **25**, 2976
 Ohira Y., Murase K., Yamazaki R., 2011, *MNRAS*, **410**, 1577
 Phaneuf R. A., Meyer F. W., McKnight R. H., 1978, *Phys. Rev. A*, **17**, 534
 Piddington J. H., 1956, *MNRAS*, **116**, 314
 Pinto C., Galli D., 2008, *A&A*, **484**, 17
 Ptuskin V. S., Soutoul A., 1990, *A&A*, **237**, 445
 Ptuskin V. S., Soutoul A., 1998, *Space Sci. Rev.*, **86**, 225
 Ptuskin V. S., Zirakashvili V. N., Plesser A. A., 2008, *Adv. Space Res.*, **42**, 486
 Reville B., Giacinti G., Scott R., 2021, *MNRAS*,
 Schroer B., Pezzi O., Caprioli D., Haggerty C., Blasi P., 2020, arXiv e-prints, p. arXiv:2011.02238
 Schultz D. R., Krstić P. S., Lee T. G., Raymond J. C., 2008, *ApJ*, **678**, 950
 Schultz D. R., Ovchinnikov S. Y., Stancil P. C., Zaman T., 2016, *J. Phys. B*, **49**, 084004
 Shah M. B., Gilbody H. B., 1985, *J. Phys. B*, **18**, 899
 Shah M. B., McCallion P., Gilbody H. B., 1989, *J. Phys. B*, **22**, 3037
 Skilling J., 1975a, *MNRAS*, **172**, 557
 Skilling J., 1975b, *MNRAS*, **173**, 255
 Squire J., Hopkins P. F., Quataert E., Kempster P., 2021, *MNRAS*, **502**, 2630
 Stancil P. C., et al., 1998, *J. Phys. B*, **31**, 3647
 Strong A. W., Moskalenko I. V., Ptuskin V. S., 2007, *Ann. Rev. Nucl. Part. Sci.*, **57**, 285–327
 Truelove J. K., McKee C. F., 1999, *ApJS*, **120**, 299
 Wentzel D. G., 1974, *ARA&A*, **12**, 71
 Wiedenbeck M. E., et al., 2007, *Space Sci. Rev.*, **130**, 415
 Wiener J., Zweibel E. G., Oh S. P., 2013, *ApJ*, **767**, 87
 Xu S., Lazarian A., Yan H., 2015, *ApJ*, **810**, 44
 Xu S., Yan H., Lazarian A., 2016, *ApJ*, **826**, 166
 Yan H., Lazarian A., 2004, *ApJ*, **614**, 757
 Zweibel E. G., Shull J. M., 1982, *ApJ*, **259**, 859

APPENDIX A: COLLISIONAL COEFFICIENTS

A1 Collisions of H^+ with H and He atoms

In the WNM and the WIM the relevant damping processes for Alfvén waves are collisions of H^+ with either H or He atoms. The case of $H^+ - H$ collisions is special because the proton elastically scattered by the H atom is indistinguishable from the recoiling proton produced by charge exchange (Krstić & Schultz 1999; Glassgold et al. 2005; Schultz et al. 2008, 2016). Therefore, the elastic scattering and the charge exchange channels for collisions of H^+ with H, as for any collision between ions and their parent gas, cannot in general be separated. Only at collision energies $E_{cm} \gg 1$ eV can the

forward elastic and the backward charge exchange be approximately separated. In this limit, $\sigma_{mt} \approx 2\sigma_{ce}$ (Dalgarno 1958), a frequently used approximation (see e.g. Kulsrud & Cesarsky 1971).

Fig. A1 shows the m.t. cross section for $H^+ - H$ collisions (Krstić & Schultz 1999; Glassgold et al. 2005), and the corresponding rate coefficient. The figure also shows the m.t. cross sections and rate coefficients derived from either charge exchange and elastic scattering in the distinguishable particle approach (Schultz et al. 2008, 2016), and the experimental determination of the m. t. cross section obtained by Brennan & Morrow (1971) by measuring the attenuation of Alfvén waves propagating in a partially-ionized hydrogen plasma at $E_{cm} \approx 5$ eV. Also shown in Fig. A1 are the rate coefficients used by Kulsrud & Cesarsky (1971) and Zweibel & Shull (1982), and frequently adopted also for other species by scaling the collision rate with the ratio m_n/m_i of the neutral and ion masses (see e.g. (Zweibel & Shull 1982)). As shown in the following, this approximation is not generally correct, since the rate coefficients in the case of other species exhibit a different dependence on the temperature compared to the $H^+ - H$ collisions case.

Fig. A2 shows the m.t. (Krstić & Schultz 1999, 2006) and c.e. (Loreau et al. 2018) cross sections for $H^+ - He$ collisions, and the corresponding rate coefficients. Charge exchange contributes to the transfer of momentum above collision energies $\sim 10^3$ eV, corresponding to relative velocities of ~ 500 km s⁻¹, much larger than typical thermal or Alfvén speeds in the WNM and WIM.

A2 Collisions of C^+ with H and He atoms

In the CNM and DiM, ion-neutral damping is dominated by the collisions between neutral hydrogen and ionized carbon. Fig. A3 shows the cross sections and reaction rates for m.t. and c.e. in the case of collisions of C^+ ions with H atoms. For collisions of C^+ ions with He atoms, no theoretical or experimental are available. The m.t. transfer rate coefficient, according to the Langevin theory, is $\langle\sigma_{mt}v\rangle_{C^+,He} = 1.33 \times 10^{-9}$ cm³ s⁻¹ (Pinto & Galli 2008). As in the case of $H^+ - He$ collisions, the large difference with the rate coefficients used in this work resides in the assumption that the rate coefficient is the same for all species.

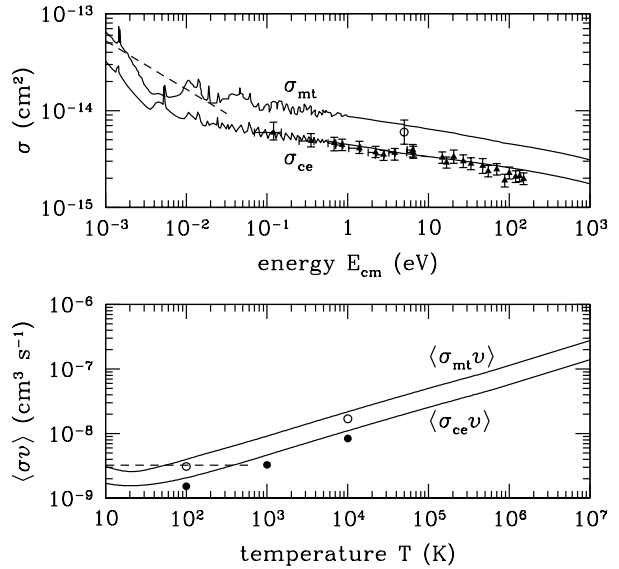


Figure A1. *Top panel:* cross sections for collisions of H^+ with H vs. collision energy in the center-of-mass frame E_{cm} . Momentum transfer cross section, from Krstić & Schultz (1999), Glassgold et al. (2005), and Schultz et al. (2008); charge exchange cross section, from Hodges & Breig (1991), and Schultz et al. (2008); *dashed line:* Langevin m.t. cross section. Experimental data for the c.e. cross section: Newman et al. (1982) (filled triangles). The empty circle shows the value of the m.t. cross section measured by Brennan & Morrow (1971) *Bottom panel:* Collisional rate coefficient for momentum transfer and charge exchange. The filled and empty circles show the rate coefficient adopted by Kulsrud & Cesarsky (1971) and Zweibel & Shull (1982), respectively.

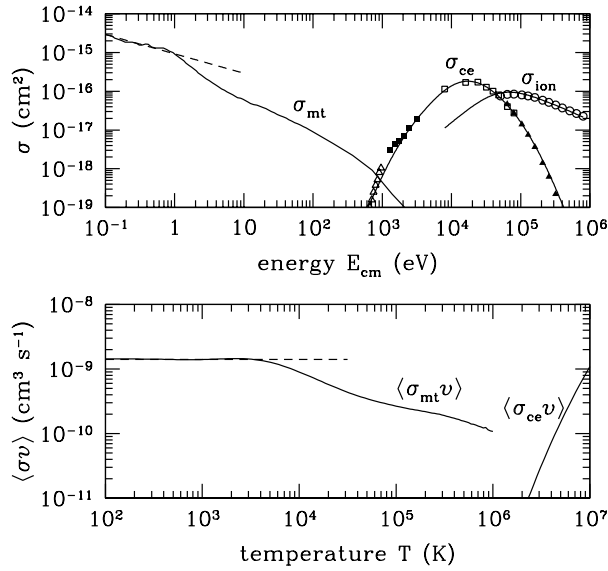


Figure A2. *Top panel:* cross sections for collisions of H^+ with He vs. collision energy in the center-of-mass frame E_{cm} . Momentum transfer cross section, from Krstić & Schultz (1999, 2006); Langevin m.t. cross section (dashed line); charge exchange cross section, from Loreau et al. (2018); and ionization cross section, from Shah & Gilbody (1985). Experimental data for the c.e. cross section: Martin et al. (1981) (empty triangles), Shah & Gilbody (1985) (filled triangles), Shah et al. (1989) (empty squares), and Kusakabe et al. (2011) (filled squares). Experimental data for the ionization cross section: Shah & Gilbody (1985) (empty circles). *Bottom panel:* Collisional rate coefficient for Langevin m.t. (dashed line), m.t. and c.e. (solid lines).

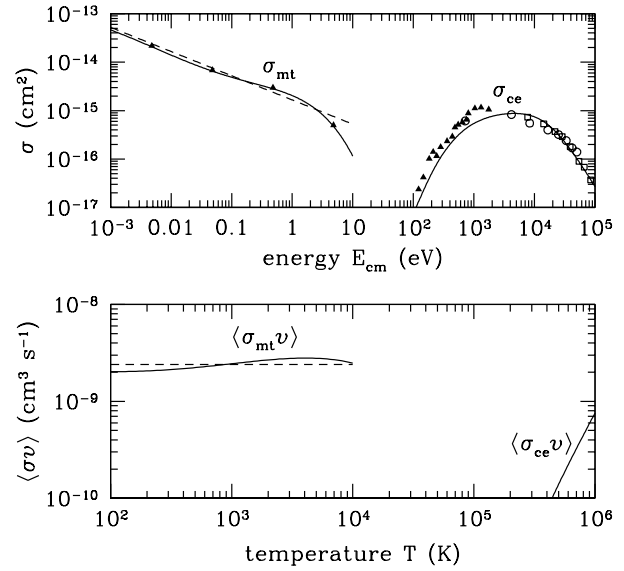


Figure A3. *Top panel:* cross sections for collisions of C^+ with H vs. collision energy in the center-of-mass frame E_{cm} : m.t. cross section computed by Flower & Pineau des Forets (1995) (filled triangles); fit, from Pinto & Galli (2008) (solid line); Langevin m.t. cross section (dashed line). Experimental data for the c.e. cross section: Phaneuf et al. (1978) (empty circles), Goffe et al. (1979) (empty squares) and Stancil et al. (1998) (filled triangles); c.e. cross section recommended by Stancil et al. (1998) (solid line). *Bottom panel:* Collisional rate coefficients: Langevin m.t. (dashed line), m.t. and c.e. (solid lines).